Application of the Jeukenne-Lejeune-Mahaux folding model to α-nucleus elastic scattering

T. Furumoto[1,*] and Y. Sakuragi[2,†]

[1]*Department of Physics, Osaka City University, Osaka 558-8585, Japan*

[2]*Department of Physics, Osaka City University, Osaka 558-8585, Japan and RIKEN, Hirosawa 2-1, Wako, Saitama 351-0198, Japan*

(Received 27 March 2006; published 28 September 2006)

A systematic analysis of α(^{4}He)-nucleus elastic scattering is made by using a microscopic optical model potential obtained by the double folding of the complex nucleon-nucleon (*NN*) effective interaction based on the *G*-matrix theory. We adopt the so-called JLM interaction as the complex *NN* interaction and test its applicability to the ^{4}He elastic scattering by ^{12}C, ^{16}O, ^{28}Si, and ^{40}Ca over a wide range of incident energy and scattering angle. The experimental cross sections for incident energies ranging from $E_{\rm lab} = 40$ to 240 MeV are well reproduced by the double folding potential up to backward angles. Although modification of the real and imaginary potential strength by about 25% and 35%, respectively, on average is necessary to reproduce the data, the renormalization factors are found to be almost constant with respect to the incident energy and target mass number.

DOI: 10.1103/PhysRevC.74.034606 PACS number(s): 21.30.Fe, 24.10.Ht, 25.55.Ci

I. INTRODUCTION

The microscopic description of a nucleus-nucleus interaction is one of the fundamental subjects in nuclear physics. In particular, it is very important to understand the complex optical potential for composite projectiles from a microscopic point of view not only to understand the relevant reaction dynamics involved but also to develop a practical tool for predicting optical potentials of colliding systems for which the elastic scattering measurement is absent or difficult, such as in the case of neutron-rich or proton-rich β-unstable nuclei. In those cases in which elastic scattering can be strongly affected by reaction channels that are strongly connected to the elastic channel, such as collective excitation channels of deformed nuclei or projectile breakup channels of loosely bound systems, there exists a strong dynamic polarization effect that has to be accounted for by, for example, coupled-channel (CC) calculations. In such cases, a microscopic interaction model serves as a tool for providing the "bare" optical potential to be used in CC calculations, rather than the net optical potential which includes the dynamic polarization effects.

The double folding model (DFM) is one of the simplest and most practical tools for constructing the interaction potential between complex nuclei. In DFM, an effective nucleon-nucleon (*NN*) interaction in nuclear medium is doubly folded with nucleon density distributions in the projectile and target nuclei. One of the most famous and successful effective *NN* interactions is the so-called M3Y *G*-matrix interaction [1] or its density-dependent version, DDM3Y one [2,3]. The DFM with the M3Y or DDM3Y interaction, however, provides us only with the real part of the nucleus-nucleus potential. In such a case, an imaginary potential must be added to the real DFM potential "by hand" to describe elastic scattering of the interacting pair. The imaginary potential is normally assumed to have some suitable functional form, such as the Woods-Saxon form or its derivative, and the potential parameters included are determined phenomenologically so as to reproduce the experimental data of elastic scattering.

For nucleon-nucleus scattering, many attempts have been made to microscopically construct the imaginary part of the optical potential, including folding model studies with the use of complex *G*-matrix interactions. For composite projectiles, however, the imaginary part of the optical potential is still treated phenomenologically in most cases, except for some pioneering works [4–6] in which complex optical potentials for light composite projectiles were constructed by DFM with the use of a complex *G*-matrix interaction proposed by Jeukenne, Lejeune, and Mahaux [7] (which we call the JLM interaction hereafter). Those works showed that the measured elastic scattering cross sections were well reproduced by the complex DFM potentials, but large reduction (renormalization) factors for both real and imaginary parts were required. However, many of the projectile nuclei investigated there were either loosely bound systems against projectile breakup, such as ^{6,7}Li and ^{7,9}Be, or β-unstable, neutron-rich or proton-rich nuclei, such as ^{11}Li and ^{17}F. For such projectiles, one would expect substantial dynamic polarization effects due to the breakup process [8] which cannot be accounted for by the folding model potential based on the effective *NN* interaction, and, hence, at least some fraction of the renormalization could originate from the dynamic effects [8]. Therefore, it is not very suitable to test the validity of the DFM itself by elastic scattering of such loosely bound projectiles.

Since application of the DFM with complex *G*-matrix interactions to composite-projectile scattering is still very limited and its applicability has not been established, it is worth testing the DFM with the JLM interaction (which we refer to as the JLM folding model in the present paper) to elastic scattering of ^{4}He, the most stable composite nucleus, on various target nuclei over a wide range of incident energy. In Ref. [4], the JLM interaction was already tested on ^{4}He elastic scattering but only for the case of a ^{12}C target at incident energies $E_{\rm lab} = 104 \sim 173$ MeV. In this paper, we apply the JLM folding model to the elastic scattering of ^{4}He on ^{12}C, ^{16}O, ^{28}Si, and ^{40}Ca target nuclei over the energy range $E_{\rm lab} = 40 \sim 240$ MeV and investigate its validity together

*Electronic address: furumoto@ocunp.hep.osaka-cu.ac.jp
†Electronic address: sakuragi@ocunp.hep.osaka-cu.ac.jp

with the possible systematics of the renormalization factors required to reproduce the experimental data.

II. JLM FOLDING MODEL

The JLM interaction is designed so that the Hartree term alone is able to reproduce the entire nucleon-nucleus optical potential in nuclear matter; hence, the interaction can be used in the folding calculation without treating the exchange component explicitly [7]. Therefore, the nucleus-nucleus potential from the JLM interaction is given by the direct term of the double folding potential [4] defined by

$$U_{\rm JLM}(\boldsymbol{R}) = \int \rho_1(\boldsymbol{r}_1)\rho_2(\boldsymbol{r}_2)v_{NN}(\boldsymbol{s};\rho, E)d\boldsymbol{r}_1 d\boldsymbol{r}_2, \quad (1)$$

where ρ_1 and ρ_2 are nucleon densities in the projectile and target nuclei, respectively, R denotes the distance between the centers of mass of the colliding nuclei, and $\boldsymbol{s} = \boldsymbol{R} + \boldsymbol{r}_1 - \boldsymbol{r}_2$ is the relative vector between interacting nucleon pair. The isoscalar part of the JLM interaction with the finite-range correction has the form [7]

$$v_{NN}(\boldsymbol{s};\rho, E) = g_R(\boldsymbol{s})V_0(\rho, E) + ig_I(\boldsymbol{s})W_0(\rho, E), \quad (2)$$

where $V_0(\rho, E)$ and $W_0(\rho, E)$ are the real and imaginary parts of the interaction strength, and their density and energy dependence are parametrized [7] in terms of polynomial forms of ρ and E as

$$V_0 = \sum_{i,j=1}^{3} a_{ij}\rho^{i-1}E^{j-1}, \quad (3)$$

$$W_0 = \left[1 + \frac{D}{(E-\epsilon_F)^2}\right]^{-1} \sum_{i,j=1}^{4} d_{ij}\rho^{i-1}E^{j-1}. \quad (4)$$

The coefficients D, a_{ij}, and d_{ij} and the definition of the Fermi energy ϵ_F are given in Ref. [7]. The finite-range form factor of the effective interaction was taken to be a single-Gaussian form

$$g_R(s) = (t_R\sqrt{\pi})^{-3}\exp(-s^2/t_R^2), \quad (5)$$

$$g_I(s) = (t_I\sqrt{\pi})^{-3}\exp(-s^2/t_I^2), \quad (6)$$

for the real part and imaginary part, respectively. The values for the range parameters are taken to be $t_R = 1.2$ fm and $t_I = 1.75$ fm following Ref. [5]. The complex DFM potential with JLM interaction is written as

$$U_{\rm JLM}(\boldsymbol{R}) = V_{\rm JLM}(\boldsymbol{R}) + iW_{\rm JLM}(\boldsymbol{R}), \quad (7)$$

where the real and imaginary parts of the DFM potential are given by

$$V_{\rm JLM}(\boldsymbol{R}) = \int \rho_1(\boldsymbol{r}_1)\rho_2(\boldsymbol{r}_2)g_R(\boldsymbol{s})V_0(\rho, E)d\boldsymbol{r}_1 d\boldsymbol{r}_2, \quad (8)$$

$$W_{\rm JLM}(\boldsymbol{R}) = \int \rho_1(\boldsymbol{r}_1)\rho_2(\boldsymbol{r}_2)g_I(\boldsymbol{s})W_0(\rho, E)d\boldsymbol{r}_1 d\boldsymbol{r}_2. \quad (9)$$

The potential strength V_0 and W_0 depend on the density ρ through Eqs. (3) and (4). In folding models, the local-density approximation (LDA) is introduced to account for the density dependence of the effective NN interaction used. Several ways of evaluating the local density are tested in the double folding procedure with the JLM interaction [4,5]. One of them is the geometric average of the individual densities,

$$\rho = \sqrt{\rho_1\left(\boldsymbol{r}_1 + \frac{\boldsymbol{s}}{2}\right)\rho_2\left(\boldsymbol{r}_2 - \frac{\boldsymbol{s}}{2}\right)}, \quad (10)$$

and the other is the arithmetic average,

$$\rho = \frac{1}{2}\left[\rho_1\left(\boldsymbol{r}_1 + \frac{\boldsymbol{s}}{2}\right) + \rho_2\left(\boldsymbol{r}_2 - \frac{\boldsymbol{s}}{2}\right)\right], \quad (11)$$

which were referred to as JLM(1) and JLM(2) in Ref. [5], respectively. In both cases, the averaged density is evaluated at the midposition of the interacting nucleons. The different prescriptions for LDA lead to slight differences in shape and central depth of the folded potential, but such minor differences cause no essential change in the calculated cross sections, as demonstrated in Ref. [5]. In fact, we have reconfirmed it in the case of ^{4}He scattering. In this paper, we adopt the geometric average but apply another type of prescription [4] for LDA

$$\rho = \sqrt{\rho_1(\boldsymbol{r}_1)\rho_2(\boldsymbol{r}_2)}, \quad (12)$$

where the local density is evaluated at each position of the interacting nucleons. This enables us to greatly reduce the computational time for numerical integrations. Again, the difference between (10) and (12) is negligible in the present case of ^{4}He elastic scattering.

III. ^{4}He ELASTIC SCATTERING

Now, we apply the JLM folding model to ^{4}He elastic scattering by ^{12}C, ^{16}O, ^{28}Si, and ^{40}Ca target nuclei for incident energies $E_{\rm lab} = 40$–240 MeV. The nucleon densities are taken from Ref. [9] for ^{4}He, Ref. [10] for ^{12}C, and Ref. [11] for ^{16}O. For ^{28}Si and ^{40}Ca, the densities are deduced from the charge densities extracted from electron-scattering experiments by unfolding the charge form factor of a proton in the standard way [9].

It is known that the JLM interaction tends to overestimate the strength of both real and imaginary parts when it is applied to the double folding model [4,5]. We then introduce renormalization factors N_V and N_W for the real and imaginary parts, respectively, and define the microscopic optical potential with the JLM interaction as

$$U_{\rm opt}(\boldsymbol{R}) = N_V V_{\rm JLM}(\boldsymbol{R}) + iN_W W_{\rm JLM}(\boldsymbol{R}) \ . \quad (13)$$

We adjust the renormalization factors so as to attain optimum fits to the experimental data for elastic scattering cross sections. We have used an automatic potential search code ALPS [12] to search for the best-fit values of the renormalization factors. We analyze ^{4}He elastic scattering by the ^{16}O target at five incident energies $E_{\rm lab} = 48.7$, 54.1, 69.5, 104, and 146 MeV; the ^{40}Ca target at six energies $E_{\rm lab} = 40.05$, 47.0, 53.9, 80.0, 104, and 140 MeV; the ^{12}C target at five energies $E_{\rm lab} = 104$, 120, 145, 166, and 172.5 MeV; and the ^{28}Si target at three energies $E_{\rm lab} = 104$, 166, and 240 MeV. The experimental data are taken from [13–20], and numerical data of the experimental cross sections are available at the

TABLE I. Values of renormalization factors for the real part N_V and for the imaginary part N_W for the folding potential with the JLM interaction obtained from optimum fits to the experimental data for ^{4}He elastic scattering by various target nuclei. Volume integrals per nucleon pair of the real and imaginary parts of the central potentials are also listed.

Target nucleus	$E_{\rm lab}$ (MeV)	N_V	N_W	$-J_V/A_PA_T$ (MeV fm^3)	$-J_W/A_PA_T$ (MeV fm^3)
^{12}C	104	0.733	0.618	326	109
	120	0.741	0.637	318	113
	145	0.729	0.638	296	112
	166	0.737	0.624	285	107
	172.5	0.721	0.636	275	108
^{16}O	48.7	0.780	0.480	383	67.8
	54.1	0.780	0.500	378	73.0
	69.5	0.750	0.630	352	98.7
	104	0.740	0.660	321	108
	146	0.740	0.680	293	113
^{28}Si	104	0.700	0.680	302	112
	166	0.705	0.670	265	108
	240	0.692	0.687	219	101
^{40}Ca	40.05	0.720	0.450	354	58.8
	47.0	0.740	0.500	359	68.4
	53.9	0.740	0.610	354	87.0
	80.0	0.700	0.650	317	102
	104	0.702	0.651	301	106
	140	0.690	0.620	274	101

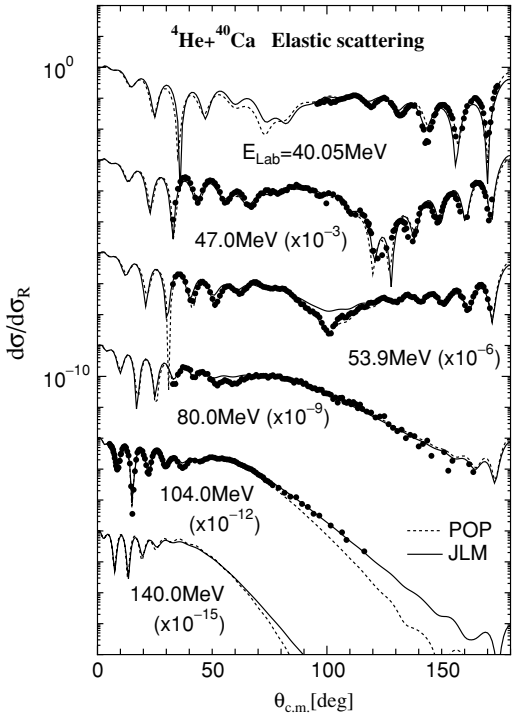

FIG. 1. Ratios of cross sections for ^{4}He elastic scattering by ^{40}Ca to the Rutherford cross sections, at $E_{\rm lab}$ = 40.5, 47.0, 53.9, 80.0, 104, and 140 MeV . Solid curves show the results of calculation with JLM folding model multiplied by renormalization factors given in Table I. Dotted curves are calculated results with best-fit POPs [20,22–24]. Experimental data are from Refs. [13,20].

nuclear data base [21], except for the $E_{\rm lab}$ = 146 MeV case on the ^{16}O target and the $E_{\rm lab}$ = 140 MeV case on the ^{40}Ca target. For these cases, we use the calculated cross sections obtained by phenomenological optical potentials which are known to reproduce well the experimental data [17,22].

The results are shown in Figs. 1–4. The solid curves show the results of best-fit JLM folding model calculation with the renormalization factors given in Table I. The values of volume integral per nucleon pair of the renormalized JLM folding model potentials are also given in the table. For ^{16}O and ^{40}Ca targets, we also compare our results with the calculated cross sections obtained by phenomenological optical potentials (POPs), which are shown by the dotted curves in Figs. 1 and 2. All the calculated cross sections reproduce well the experimental data up to the most backward angles, with about 25 $\sim$ 30% renormalization (reduction) to the real part and about 35% to the imaginary part of the JLM folding potential.

The precise reproduction of characteristic oscillatory patterns at the middle and backward angles of experimental cross sections for the low-energy scattering by ^{16}O and ^{40}Ca targets is particularly impressive. The large bump at middle angles followed by a deep minimum and a rapid oscillation at backward angles are typical features of refractive scattering of an α particle which penetrates into the deep interior of nuclear potential and is deflected toward backward angles, known as the nuclear rainbow phenomenon and the anomalous large-angle scattering (ALAS). This kind of refractive scattering is known to precisely probe the detailed shape and depth of the nuclear potential over the entire radial range. Therefore,

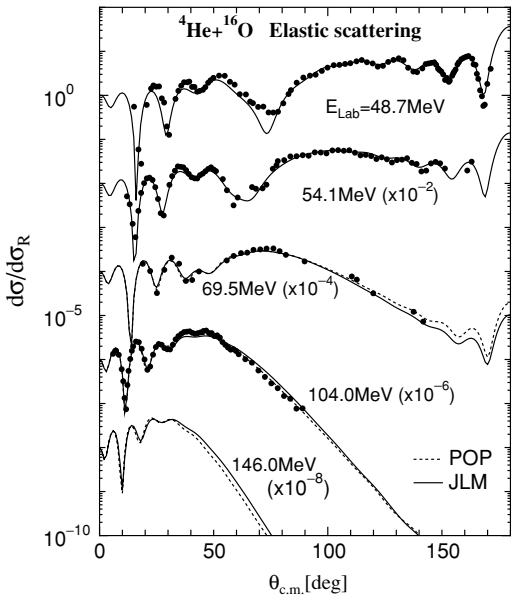

FIG. 2. Same as Fig. 1, but for ^{4}He elastic scattering by ^{16}O at $E_{\rm lab}$= 48.7, 51.4, 69.5, 104, and 146 MeV. Experimental data are from Refs. [13,16,17]. Dotted curve for 146 MeV is the calculated result with best-fit POPs [17].

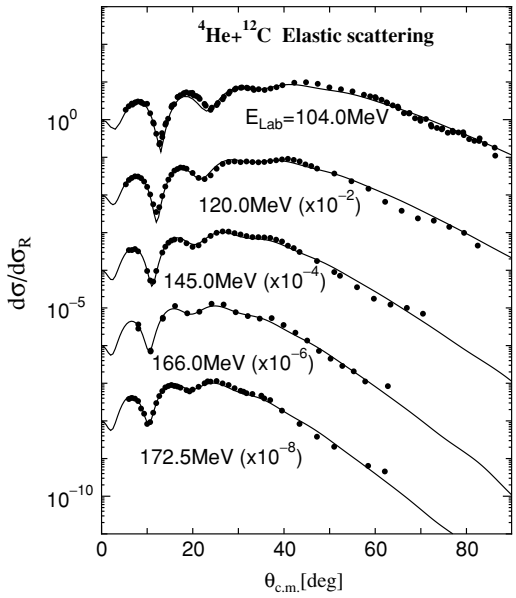

FIG. 3. Same as Fig. 1, but for ^{4}He elastic scattering by ^{12}C at E_{lab} = 104, 120, 145, 166, and 172.5 MeV. Experimental data are from Refs. [13–15].

precise reproduction of this refractive scattering by the present JLM folding model calculation implies that the folding model predicts precise shapes of the real part as well as the imaginary part of the optical potential consistent with the observed refractive phenomena, although the strength of the folding potential has to be renormalized.

As examples, we show the comparison between the (renormalized) JLM folding model potentials and the POPs in the cases of ^{4}He+^{16}O scattering at E_{lab} = 69.5, 104 and 146 MeV in Fig. 5 and ^{4}He+^{40}Ca scattering at E_{lab} = 47.0, 80.0, and 104 MeV in Fig. 6. The shape of the real and imaginary parts of POP is well reproduced by the JLM folding model.

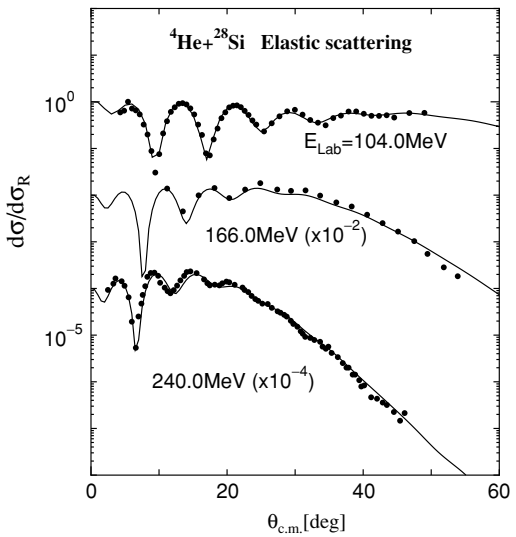

FIG. 4. Same as Fig. 1, but for ^{4}He elastic scattering by ^{28}Si at E_{lab} = 104, 166, and 240 MeV. Experimental data are from Refs. [13,15,19].

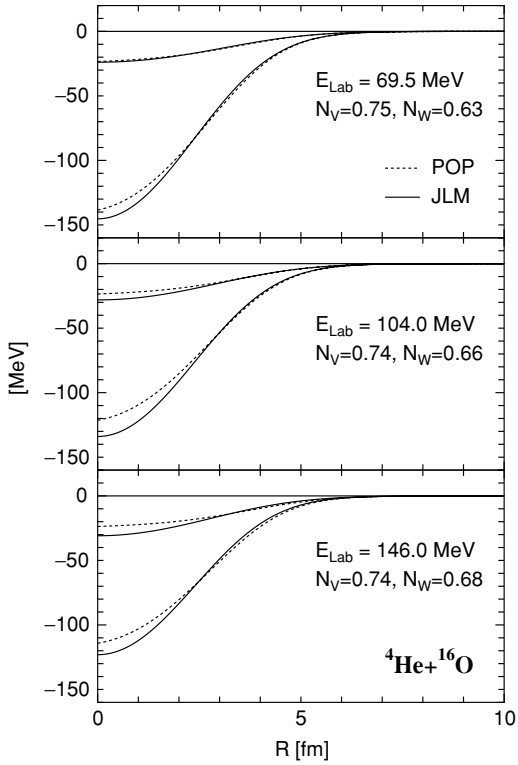

FIG. 5. Comparison of JLM folding potential with a best-fit POP [17] for ^{4}He scattering by ^{16}O at E_{lab} = 69.5, 104, and 146 MeV. Real and imaginary parts of the folding potentials for each E_{lab} are multiplied by renormalization factors N_V, N_W.

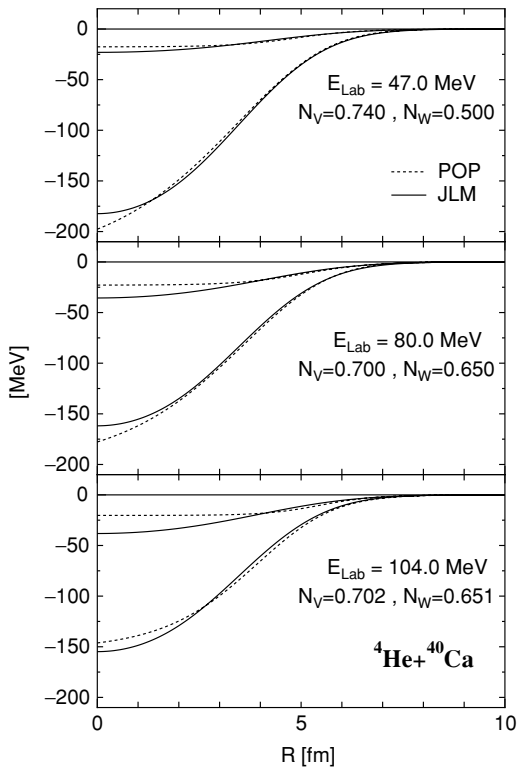

FIG. 6. Same as Fig. 5, but for scattering by ^{40}Ca at E_{lab} = 47.0, 80.0, and 104 MeV. POPs for E_{lab} = 47.0, 80.0 MeV are from Ref. [20], and that for 104 MeV is from Ref. [24].

Particularly, in the cases of 69.5 MeV scattering by ^{16}O and 47.0 MeV scattering by ^{40}Ca, two kinds of potentials are almost identical in both real and imaginary parts, as seen in Figs. 5 and 6, which is consistent with almost perfect fits to the experimental data up to backward angles, as seen in Figs. 1 and 2.

The difference between folding potential and POP becomes noticeable as we go to higher energies, especially in the case of the ^{40}Ca target, as seen in Fig. 6. However, it should be noted that the imaginary potential becomes stronger as the incident energy increases; hence, cross sections, even at backward angles, become less sensitive to fine details of the potential at short distances because of the increase of absorption at higher energies. In other words, there exists uncertainty in the depth and shape of the POP itself, particularly at short distances, as discussed in Ref. [20] based on the analysis using a model-independent shape for the optical potential, such as the sum-of-Gaussian (SOG) form. In addition, a noticeable difference in shape for the imaginary part at short distances between POP (dotted curves) and the folding potentials (solid curves), seen in the case of $E_{\rm lab} = 80.0$ and 104 MeV on the ^{40}Ca target, may partly be due to a restricted functional form (the Woods-Saxon form in these cases) adopted for the imaginary part of POP [20,24]. In fact, a more suitable functional form, the squared Woods-Saxon form, was adopted for the real part of POP (dotted curves for the real part of $E_{\rm lab} = 80.0$ and 104 MeV potentials in Fig. 6) as well as for the real and imaginary parts of POP for the ^{16}O target [17] (dotted curves in Fig. 5) which are much closer to the shape of folding potentials.

Next, we compare in Figs. 7 and 8 the volume integral per nucleon pair, J_V/A_PA_T and J_W/A_PA_T, for the real and imaginary parts of the folding potential and POP [20,22–24], as a function of incident energy per nucleon ($E_{\rm lab}/A_P$) for each target nucleus. For ^{16}O and ^{40}Ca targets, we also plot the values obtained by the folding potential with the use of the DDM3Y effective *NN* interaction for the real part, which are also multiplied by renormalization factors given in [16,25]. In each figure, the solid and dotted curves show the energy dependence of J_V/A_PA_T and J_W/A_PA_T for the JLM folding model potential multiplied by a constant renormalization factor shown in each figure. It is seen that most values obtained by the optimum fits to the experimental data at each energy (solid circles and solid squares) lie closely to the curve with a constant renormalization factor at energies higher than $E_{\rm lab}/A_P \simeq 20$ MeV. This allows us to expect that the JLM folding model with constant renormalization is able to predict correct optical potentials for ^{4}He elastic scattering for incident energies of $E_{\rm lab}/A_P \geqslant 20$ MeV.

For $E_{\rm lab}/A_P \leqslant 20$ MeV, however, as shown only in the cases of ^{16}O and ^{40}Ca targets, both the real and imaginary potentials start to deviate from the uniform curves extrapolated from the higher energy side. Namely, the imaginary part rapidly decreases as the incident energy decreases, while the real part has slightly larger values than the solid curve of a constant renormalization factor and tends to show a bell-shape-like behavior, which is more clearly seen in the case of the ^{40}Ca target. This trend is not limited to the present JLM folding model but is common to all types of optical potentials, as

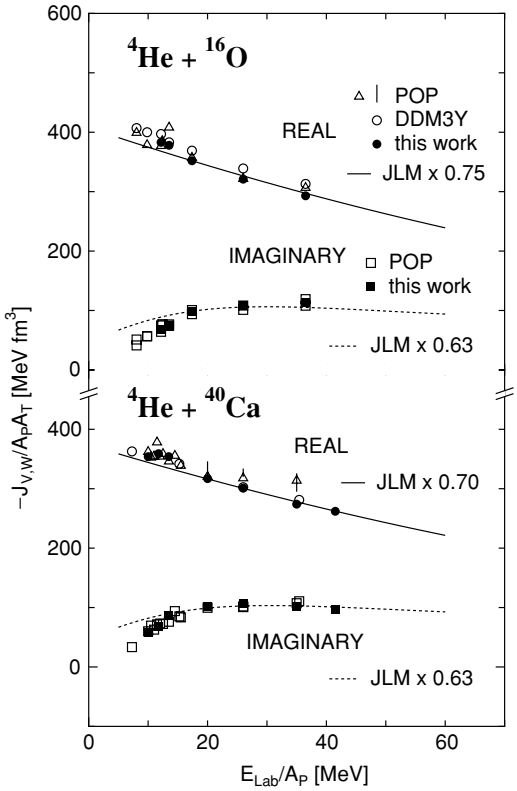

FIG. 7. Energy dependence of the real and imaginary parts of the volume integral per nucleon pair of optical potentials for the ^{4}He-^{16}O and ^{4}He-^{40}Ca systems. Solid circles (solid squares) for the real (imaginary) part are values of the present JLM folding potential multiplied by a renormalization factor given in Table I. Open triangles (open squares) for ^{4}He-^{16}O are of the real (imaginary) part of POP [17], while open triangles and vertical bars (open squares) for ^{4}He-^{40}Ca are of the real (imaginary) part of POP [20,22–24]. Open circles for the real part are of the folding potentials with the DDM3Y interaction, which are also multiplied by renormalization factors given in [16,25]. Solid and dotted curves show the energy dependence of J_V/A_PA_T and J_W/A_PA_T for the JLM folding model potential multiplied by a constant renormalization factor.

clearly seen in the figures. This kind of anomalous behavior of optical potentials is known as the "threshold anomaly" [26] which is widely observed in optical potentials not only of α particles but also of nucleon and various heavy ions near the Coulomb-barrier energies. The threshold anomaly occurs mainly because of an effective closure of open reaction channels that occurs when the incident energy drops below the effective Coulomb barrier of the colliding system. This anomaly is well explained in terms of the "dispersion relation" [27] which holds between the real and imaginary parts of the generalized optical potential. That is, the present JLM folding model is unable to reproduce the effective closure of reaction channels below the Coulomb barrier energies, although it should be noted that the imaginary part of the JLM folding potential also shows a slight decrease toward the lower energy side, as seen in Figs. 7 and 8.

The characteristic behavior of optical potential as a function of incident energy is more clearly observed in the energy

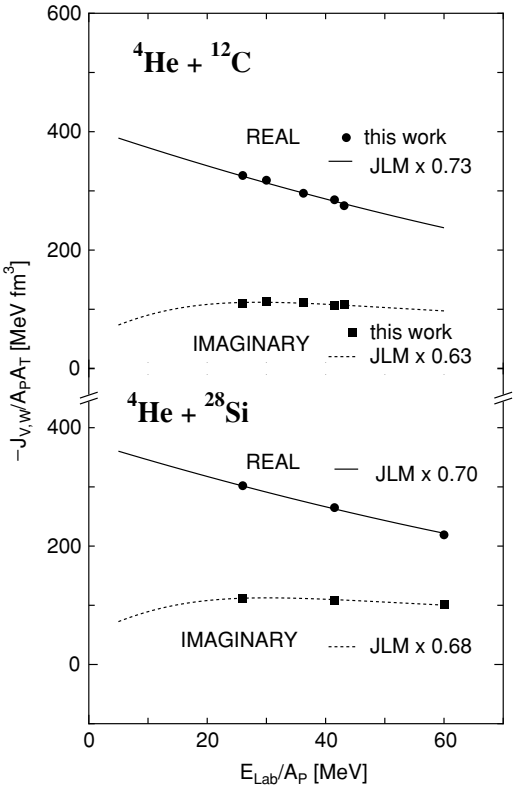

FIG. 8. Same as Fig. 7, but for the ^{4}He-^{12}C and ^{4}He-^{28}Si systems. Solid circles (solid squares) for the real (imaginary) part are values of the present JLM folding potential multiplied by a renormalization factor given in Table I.

dependence of renormalization factors for the present JLM folding potential, N_V and N_W, as shown in Fig. 9 in the case of the ^{40}Ca target. It is clearly seen that a rapid decrease of N_W toward the lower energy side correlates well with the bell-shape deviation of N_V from the constant line (solid line), which shows a typical behavior of the dispersion relation between the real and imaginary parts of the dynamic polarization component of the optical potential [26,27].

The target-mass dependence of the renormalization factors is shown in Fig. 10 in the case of $E_{\rm lab} = 104$ MeV. It is seen that the renormalization factors slightly depend on the target mass number. The values are close to the average values of $N_V = 0.71$ and $N_W = 0.63$, except for N_W for the ^{28}Si target, for which the value visibly deviates from the average line. It is noticed from Table I and Fig. 8 that N_W for the ^{28}Si target has slightly larger values also for other incident energies, which may suggest that the ^{28}Si nucleus presents a slightly stronger absorption to the incident α particle compared with other target nuclei, two of which are closed-shell nuclei. Since the ^{28}Si nucleus is known to be a very deformed nucleus that shows a typical rotational band, it may be reasonable to expect that an additional absorption should be induced dynamically by collective excitations, such as the collective rotation, of the ^{28}Si nucleus in the collision with ^{4}He. This kind of dynamic effect may not be included in the imaginary part originated from the G-matrix interaction evaluated in nuclear matter.

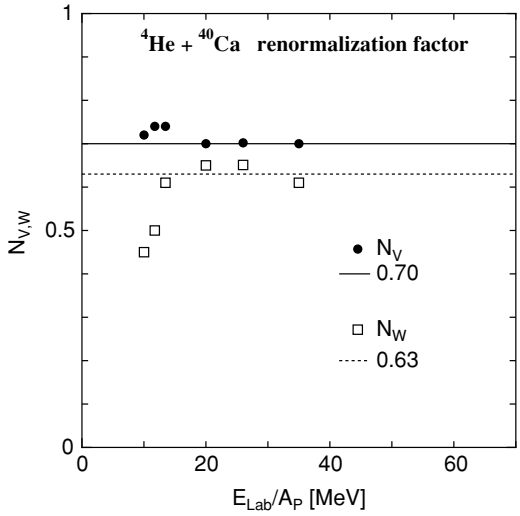

FIG. 9. Energy dependence of renormalization factor for JLM interaction deduced from the optimum fits to ^{4}He+^{40}Ca scattering. Solid circles show N_V; open squares N_W. Solid and dotted lines show their constant values. Abscissa denotes the incident energy per nucleon ($A_P = 4$).

As we have seen in Table I, the values of the renormalization factor required to reproduce the experimental data are almost constant, $N_V \simeq 0.70 \sim 0.75$ and $N_W \simeq 0.65$, in the energy range of $E_{\rm lab}/A_P \geqslant 20$ MeV. Although the constant values depend slightly on the target, this indicates that the JLM folding model has a predicting power on the ^{4}He elastic scattering by nuclei at least for $E_{\rm lab}/A_P \geqslant 20$ MeV domain. Namely, one can expect that the complex optical potential obtained by the JLM folding model multiplied by renormalization factors of $N_V \simeq 0.70 \sim 0.75$ and $N_W \simeq 0.65$ to the real and imaginary parts, respectively, generates correct elastic scattering cross sections. Below the energy domain, the dynamic effect of an effective closure of open reaction channels becomes evident,

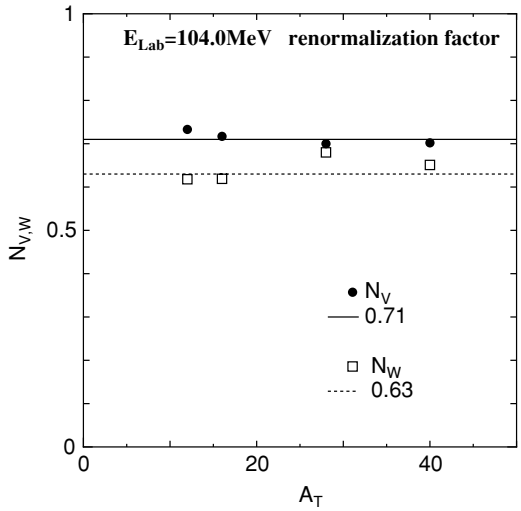

FIG. 10. Target mass dependence of renormalization factor for JLM interaction. Solid circles and open squares show N_V and N_W, respectively; solid and dotted lines show their constant values.

and, hence, the dynamic correction has to be added to the folding potentials.

IV. SUMMARY AND DISCUSSION

In the present paper, we apply the JLM folding model to elastic scattering of α particles (^{4}He) by ^{12}C, ^{16}O, ^{28}Si, and ^{40}Ca at incident energies of $E_{\rm lab} = 40$–240 MeV. All the experimental cross sections are reproduced surprisingly well by the double folding potential up to backward angles. The shape of the real and imaginary part of phenomenological optical potentials is well reproduced by the JLM folding model over the entire radial range, although the strengths of the real and imaginary parts have to be reduced by about 25% and 35%, respectively, on average. The renormalization factors are found to be almost constant with respect to the incident energy and target mass number, except for very low incident energies below the effective Coulomb barrier of the colliding system or for the ^{28}Si target having a large deformation. This may suggest that the JLM folding model has a predicting power of the complex optical potential for nucleus-nucleus scattering above Coulomb barrier energies, as long as the projectile and/or target nuclei suffer from no strong collective excitation, such as the rotation of a largely deformed nucleus or the breakup of a weakly bound system. The collective excitations of colliding nuclei generate a large amount of correction (dynamic polarization potential) which should be added to the folding potential obtained by the G-matrix interaction. In other words, the JLM folding model with a suitable constant renormalization can serve as the so-called bare optical potential to be used in coupled-channel calculations which explicitly treat the coupling to strong excitation channels. It is, therefore, very interesting to apply the JLM folding model to coupled-channel calculations for systems having strong excitation channels, including the breakup ones, and to test its validity as a practical interaction model for generating complex bare optical potentials.

A large deviation of the volume integral per nucleon pair in the sub-Coulomb barrier region from smooth curves extrapolated from the high energy region, as seen in Fig. 7, demonstrates a typical behavior of the so-called threshold anomaly which can be well accounted for by the dispersion relation [26,27] between the real and imaginary parts of optical potential. A large deviation of the renormalization factor N_W from a constant value (seen in Fig. 9) indicates that the rapid decrease of imaginary potential below the Coulomb barrier cannot be reproduced by the intrinsic energy dependence of the JLM folding model.

The defect in the sub-Coulomb barrier region may not be limited to the present JLM folding model but may be common to any folding model based on G-matrix interactions, because the rapid decrease of imaginary potential strength at the sub-Coulomb barrier region reflects, at least partly, the finite size of the colliding nuclei. The finite size of the nuclei may give rise to two effects on the imaginary potential, which are absent in the nuclear matter evaluation. The first one may simply be the existence of the Coulomb barrier between composite nuclei, and below the Coulomb barrier little incident flux can penetrate into the nuclear interaction region, which strongly suppresses the nuclear reactions from occurring at subbarrier energies. Another finite-size effect may be a discrete excitation spectrum of the colliding nuclei and resultant low level density, particularly at the low-excitation energy region. This is in contrast with the case of nuclear matter which has a continuous excitation spectrum outside the Fermi sphere. The discreteness and low level density may suppress nuclear excitations from occurring at low incident energies for which the average excitation energy is rather low compared to high-energy collisions. Therefore, it is reasonable that the imaginary potential obtained by the folding model calculation with a G-matrix interaction should be stronger compared with the realistic optical potential for a finite nuclear system in the sub-Coulomb barrier region.

On the other hand, for high-energy collisions, the average excitation energy must be high enough so that the major part of the excitation spectrum can be regarded as an almost continuous one similar to that of the nuclear matter; hence, the imaginary potential estimated by the folding model with G-matrix interactions should give a good account of the imaginary potential for the finite nuclear system.

The need for considerable renormalization $N_W \simeq 0.65$ to the imaginary part of the present JLM folding potential even in the high-energy region seems to contradict the above discussion. However, this may not necessarily imply that the JLM interaction itself largely overestimates the imaginary part. It is more likely that the need for about 35% reduction of the imaginary strength (and about 25% reduction of the real part also) may be closely related to the adopted prescription for evaluating the local density in the double folding model (DFM) calculation of the nucleus-nucleus potential.

Since the JLM interaction (and many other effective interactions) is originally designed to be used for constructing the nucleon-nucleus potentials in a single-folding model calculation, its density dependence is parametrized so as to be valid only for densities less than the saturation density ρ_0 of nuclear matter. However, its application to the DFM calculation for nucleus-nucleus potential is not as straightforward because no unique prescription for evaluating the local density has been established.

In the present paper, and in many other works that used the JLM interaction, the local density was evaluated either by the geometric average [Eqs. (10) or (12)] or the arithmetic one [Eq. (11)] of ρ_1 and ρ_2, because, and so that, the averaged density (either geometric or arithmetic) does not exceed ρ_1 or ρ_2 or, hence, the saturation density ρ_0. As already mentioned, no essential difference in the calculated ^{4}He-target DFM potential was observed between different prescriptions given in Eqs. (10)–(12), as long as we adopted the "average prescription" for evaluating the local density. However, the average prescription clearly underestimates the density effects as compared with another type of prescription, called the "frozen density prescription,"

$$\rho = \rho_1 + \rho_2, \tag{14}$$

which is also widely used in DFM calculations with DDM3Y [3] or similar types of effective interactions [28]. The problems connected with the choice of a prescription for evaluating the

local density were also discussed (but only for the real part of the potential) in an early paper [29] making use of the JLM interaction.

Although no clear answer is available to the question of which type of prescription for evaluating the local density is correct or reasonable, the "underestimation" of the local density in the average prescription [Eqs. (10)–(12)] with respect to the frozen density one [Eq. (14)] apparently leads to a relatively deeper potential because the strength of the usual effective *NN* interactions evaluated by the *G*-matrix theory increases with the decrease of density. Therefore, one might expect that if the frozen density prescription is adopted, one could obtain a much weaker folding potential for the ^{4}He-nucleus system, and the optimum renormalization factors N_V and N_W could possibly be close to unity.

However, as already pointed out [4,29], the extension of the JLM interaction to the domain of density higher than the saturation density ρ_0, above which the JLM parametrization is no longer valid, leads to the unrealistic strength of both the real and imaginary parts of the DFM potential at short distances where the local density evaluated by the frozen density prescription largely exceeds the saturation density ρ_0. The unrealistic, strange behavior of the folding potential in the high-density region is, however, mainly due to the polynomial forms [Eqs. (3) and (4)] adopted for parametrizing the density dependence of the JLM interaction in the original paper [7] and may not be due to an essential defect or invalidness of the JLM interaction itself in the high-density region. Therefore, a possible improvement of parametrization for the ρ dependence of the JLM interaction to make it applicable to the higher density domain could enable us to apply the frozen density prescription in the DFM calculation with the JLM interaction. Such an improvement could, at least partly, resolve the substantial renormalization problem observed in the present paper in the case of ^{4}He-nucleus scattering and similar problems observed in applications to other heavy-ion scattering [4–6]. A study in this direction is under way by the present authors.

ACKNOWLEDGMENTS

The authors would like to thank Professor Y. Iseri for valuable discussions about the JLM folding model and for allowing them to use the ALPS computer code for the optimum potential research done in this work.

[1] G. Bertsch, J. Borysowicz, H. McManaus, and G. R. Satchler, Nucl. Phys. **A284**, 399 (1977).
[2] G. R. Satchler and W. G. Love, Phys. Rep. **55**, 183 (1979).
[3] M. El-Azab Farid and G. R. Satchler, Nucl. Phys. **A438**, 525 (1985).
[4] F. Carstoiu and M. Lassau, Nucl. Phys. **A597**, 269 (1996).
[5] L. Trache, A. Azhari, H. L. Clark, C. A. Gagliardi, Y. W. Lui, A. M. Mukhamedzhanov, R. E. Tribble, and F. Carstoiu, Phys. Rev. C **61**, 024612 (2000).
[6] J. C. Blackmon *et al.*, Phys. Rev. C **72**, 034606 (2005).
[7] J. P. Jeukenne, A. Lejeune, and C. Mahaux, Phys. Rev. C **16**, 80 (1977).
[8] Y. Sakuragi, Phys. Rev. C **35**, 2161 (1987).
[9] L. R. B. Elton, *Nuclear Size* (Oxford University, Oxford, 1961).
[10] M. Kamimura, Nucl. Phys. **A351**, 456 (1981).
[11] J. W. Negele, Phys. Rev. C **1**, 1260 (1970).
[12] Y. Iseri, computer code ALPS (unpublished).
[13] G. Hauser, R. Lohken, H. Rebel, G. Schatz, G. W. Schweimer, and J. Specht, Nucl. Phys. **A128**, 81 (1969).
[14] S. Wiktor, C. Mayer-Boricke, A. Kiss, M. Rogge, P. Turek, and H. Dabrowski, Acta Phys. Pol. B **12**, 491 (1981).
[15] I. Brissaud, M. K. Brussel, M. Sowinski, and B. Tatischeff, Phys. Lett. **B30**, 324 (1969).
[16] H. Abele, H. J. Hauser, A. Korber, W. Leitner, R. Neu, H. Plappert, T. Rohwer, G. Staudt, M. Strasser, S. Welte, M. Walz, P. D. Eversheim, and F. Hinterberger, Z. Phys. A **326**, 373 (1987).
[17] F. Michel, J. Albinski, P. Belery, Th. Delbar, Gh. Gregoire, B. Tasiaux, and G. Reidemeister, Phys. Rev. C **28**, 1904 (1983).
[18] H. Rebel, G. W. Schweimer, G. Schatz, J. Specht, R. Lohken, G. Hauser, D. Habs, and H. Klewe-Nebenius, Nucl. Phys. **A182**, 145 (1972).
[19] D. H. Youngblood, Y. W. Lui, and H. L. Clark, Phys. Rev. C **65**, 034302 (2002).
[20] H. P. Gubler, U. Kiebele, H. O. Meyer, G. R. Plattner, and I. Sick, Phys. Lett. **B74**, 202 (1978); Nucl. Phys. **A351**, 29 (1981).
[21] Nuclear Data Base on www-nds.iaea.org (1999–2005).
[22] D. A. Goldberg, Phys. Lett. **B55**, 59 (1975).
[23] Th. Delbar *et al.*, Phys. Rev. C **18**, 1237 (1978).
[24] H. J. Gils, E. Friedman, H. Rebel, J. Buschmann, S. Zagromski, H. Klewe-Nebenius, B. Neumann, R. Pesl, and G. Bechtold, Phys. Rev. C **21**, 1239 (1980).
[25] U. Atzrott, P. Mohr, H. Abele, C. Hillenmayer, and G. Staudt, Phys. Rev. C **53**, 1336 (1996).
[26] C. Mahaux, H. Ngô, and G. R. Satchler, Nucl. Phys. **A449**, 354 (1986).
[27] M. A. Nagarajan, C. C. Mahaux, and G. R. Satchler, Phys. Rev. Lett. **54**, 1136 (1985).
[28] D. T. Khoa, G. R. Satchler, and W. von Oertzen, Phys. Rev. C **56**, 954 (1997).
[29] F. Duggan, M. Lassaut, F. Michel, and N. Vinh Mau, Nucl. Phys. **A355**, 141 (1981).